Demonstration of gate control of spin splitting in a high-mobility InAs/AlSb two-dimensional electron gas

B. Shojaei, P. J. J. O'Malley, J. Shabani, P. Roushan, B. D. Schultz, R. M. Lutchyn, C. Nayak, J. M. Martinis, and C. J. Palmstrøm

Phys. Rev. B **93**, 075302 — Published 1 February 2016

DOI: 10.1103/PhysRevB.93.075302

Demonstration of gate control of spin-splitting in a high mobility InAs/AlSb two-dimensional electron gas

B. Shojaei[1], P. J. J. O'Malley[2], J. Shabani[3], P. Roushan[2], B. D. Schultz[4], R. M. Lutchyn[5], C. Nayak[5], J. M. Martinis[2], and C. J. Palmstrøm[1, 3, 4, a]

1. *Materials Department, University of California, Santa Barbara, CA 93106, USA*
2. *Department of Physics, University of California, Santa Barbara, CA 93106, USA*
3. *California NanoSystems Institute, University of California, Santa Barbara, CA 93106, USA*
4. *Department of Electrical and Computer Engineering, University of California, Santa Barbara, CA 93106, USA*
5. *Microsoft Research, Station Q, University of California, Santa Barbara, CA 93106, USA*

Abstract

Control of zero field spin-splitting is realized in a dual-gated high quality InAs-AlSb two-dimensional electron gas. Magnetotransport experiments showed clean Shubnikov-de Haas oscillations down to low magnetic fields, and the gate-tuned electron mobility exceeded 700,000 cm^2/Vs. A clear beating effect was observed in magnetoresistance oscillations at large potential asymmetry between gates. Beat patterns due to zero field spin-splitting and other classes of transverse magnetoresistance oscillations were distinguished by temperature dependent magnetoresistance measurements. Analysis of the magnetoresistance oscillations indicated the zero field spin-splitting could be tuned via the Rashba effect while keeping the two-dimensional electron gas charge density constant.

---

a) Electronic mail: cpalmstrom@ece.ucsb.edu

Manuscript

Bychkov and Rashba's description of the lifting of spin degeneracy by spin-orbit interaction in two-dimensional semiconductors[1] has inspired numerous predictions and discoveries regarding the nature of carrier spin in semiconductor heterostructures. Control over spin-orbit interaction in semiconductors is necessary for developing novel spin-based electronics[2–4] and studying phenomena mediated by spin-orbit coupling[5], which include spin filtering techniques[6,7], spin-orbit qubits[8,9], all-semiconductor spin-FETs[10,11], and topological superconductivity in semiconductor-superconductor heterostructures[12–15]. In addition to strong spin-orbit coupling, low-dimensional systems require sufficiently high carrier mobility to enable their utilization for quantum information processing[16]. Experimental and technological advances require semiconductor materials that are low in disorder and provide a large degree of control over the spin-splitting energy.

A powerful mechanism that evokes spin-splitting of electronic energy bands uses a combination of inversion asymmetry and spin-orbit interaction. In non-centrosymmetric zinc-blende semiconductors, such as InAs, the lack of an inversion center of symmetry results in a built-in electric field which from the reference frame of a mobile carrier appears as a magnetic field. The bulk inversion asymmetry produces a splitting in both conduction and valence band states mediated by spin-orbit interaction and is referred to as the Dresselhaus effect[17]. Heterostructures of such materials have additional symmetry breaking internal electric fields and accommodate the application of an external electric field. The structure inversion asymmetry in heterostructures induces an additional energy splitting of spin-degenerate subbands and is referred to as the Rashba effect[1]. The spin-splitting energy due to the Rashba effect in narrow gap semiconductor heterostructures is comparable to or exceeds the spin-splitting energy that

results from the Dresselhaus effect[18]. The magnetic field generated by the Rashba effect is proportional to the expectation value of the electric field within the confinement potential, and the Dresselhaus field is inversely proportional to the thickness of the confined material[19]. The Rashba effect allows the use of an insulated electrostatic gate to modify the electric field over the heterostructure, and in turn, control the spin-splitting energy of the electronic energy bands.

Control over the spin-orbit coupling has been demonstrated in several heterostructures of zinc-blende semiconductors. The Rashba effect was used to control the spin-orbit coupling in an InAs/InAlAs heterostructure using an external gate voltage[20]. The contribution to the spin-splitting energy from asymmetric wave function penetration into barriers was experimentally observed in an asymmetric InAs/InGaAs quantum well[21]. In these experiments, the spin splitting energy was quantified by analyzing the beat patterns in Shubnikov-de Haas (SdH) oscillations. Weak antilocalization analysis of low field magnetoresistance was used to determine the spin splitting energy in asymmetrically doped InAs/InAlAs heterostructures[22]. A gate controlled transition from weak antilocalization to localization allowed the distinction between Rashba, as well as linear and cubic Dresselhaus contributions to the total spin-orbit field in a GaAs heterostructure[23]. In these systems, experimental findings have corroborated theoretical predictions. In contrast, in heterostructures where InAs was confined by AlSb barriers conflicting results have been reported on the ability to control the spin-orbit coupling via modifications to heterostructure asymmetry. Notably, modification of the spin splitting energy was solely attributed to a change in the Fermi wave vector in an insulated gate structure[24]. In addition magnetotransport measurements showed a lack of a beat pattern in Shubnikov-de Haas oscillations in 2DEGs wherein the carrier density and with it the self-consistent electric field

were varied by the persistent photoconductivity effect[25]. The nature of spin-splitting in InAs/AlSb heterostructures has remained ambiguous.

In this work the gate control of spin-orbit coupling is demonstrated in a 2DEG confined to an unintentionally doped InAs/AlSb heterostructure. The high quality of the 2DEG and the integration of both a front and back gate resulted in a gate-tuned electron mobility exceeding 700,000 cm^2/Vs. A low magnetic field onset of magnetoresistance oscillations enabled a Fourier analysis of SdH oscillations with high frequency resolution. Beat patterns in the SdH oscillations formed at large potential asymmetry between front and back gates. Beat patterns due to zero-field spin-splitting and magneto-inter-subband scattering were distinguished by temperature dependent magnetoresistance measurements. Analysis of the magnetoresistance oscillations indicated the spin-splitting energy in the first subband depended strongly on the asymmetry induced by the two gates. The analysis was implemented over a wide carrier density regime in this system and determined the spin-splitting energy could be controlled by the Rashba effect while keeping the 2DEG charge density constant.

The heterostructure was grown by molecular beam epitaxy (MBE) on a GaSb:Te (001) substrate mounted to a molybdenum substrate holder using gallium. Prior to the growth of the heterostructure the oxide was thermally desorbed under atomic hydrogen in a custom ultra-high-vacuum preparation chamber with a base pressure of 2×10^{-10} mbar. During the 30 minute desorption procedure, the chamber pressure was maintained at 3×10^{-6} mbar by adjusting the hydrogen flow rate through an atomic hydrogen source operating at 1900 °C. The substrate temperature, measured by a thermocouple, was maintained at 500 °C. Following oxide desorption, the substrate was transferred *in-situ* to a modified VG V80H for the growth of the heterostructure.

In a previous work it was reported that carrier mobility and single particle lifetime in InAs/(Al,Ga)Sb heterostructures are sensitive to the dislocation density in the epitaxial layers[26]. Therefore, the growth proceeded with a 20 nm GaSb buffer and a 200 nm $AlAs_{0.09}Sb_{0.91}$ epitaxial film to act as an electrically isolating, lattice matched buffer between the conductive GaSb:Te substrate and the InAs channel. After the $AlAs_{0.09}Sb_{0.91}$ buffer the growth proceeded with a ten period 2.5 nm AlSb x 2.5 nm GaSb superlattice, over the course of which reflection high energy electron diffraction oscillations were monitored to verify calibrated growth rates and a layer by layer growth mode for both AlSb and GaSb. Following the superlattice the growth proceeded with a 30 nm AlSb bottom barrier, a 15 nm InAs channel, and a 50 nm AlSb top barrier. The interfaces between the InAs channel and the barriers were formed using a shutter sequence developed by Tuttle[27]. The structure was terminated with a 3 nm GaSb capping layer to prevent the oxidation of the Al-containing layers. A schematic of the heterostructure is shown in figure 1a.

The surface of the MBE grown film appeared flat when examined under a Nomarski microscope at 100x magnification. Atomic force microscopy (AFM) of the surface revealed height variations corresponding to GaSb monolayer-height steps (0.3 nm). The root-mean-square roughness[28] of the 5 μm x 5 μm AFM image shown in figure 1b is 0.18 nm.

A gated Hall bar device with dimensions 80 μm x 20 μm was fabricated using standard microfabrication techniques. Following mesa definition by wet chemical etching, 50 nm of Al_2O_3 was grown by atomic layer deposition to serve as the top gate dielectric. To avoid an electrical short to the substrate, openings for the ohmic contacts were formed by first etching vias through the gate dielectric, then through the top antimonide barrier and stopping on the InAs channel.

Ti/Au was deposited by electron beam evaporation to serve as both ohmic and gate metallization. An optical micrograph of the device is shown in figure 1c.

Longitudinal resistance was measured in the [1-10] crystallographic direction. Measurements were performed at cryogenic temperatures in a He-4 cryostat using standard lock-in techniques under an excitation current of 1 μA. The 2DEG carrier density varied linearly under both back and front gate operation.

The integration of a front and back gate allowed independent control of the electric field over the quantum well and the 2DEG carrier density. A self-consistent calculation of the Schrodinger and Poisson equations[29] allowed the study of the conduction and valence band profiles, carrier density distributions, and the expectation value of the electric field over the quantum well in the gated hall bar device under gate operation. Band parameters reported by Vurgaftman et al.[30] were used for the III-V heterostructure, and parameters reported by Huang et al.[31] were used for the ALD grown Al_2O_3 gate dielectric. The conduction band profile and carrier density distribution in the vicinity of the InAs channel for two combinations of front and back gate voltages are depicted in figure 1d. The origin of the growth axis was chosen to be the interface of the GaSb capping layer and the Al_2O_3 gate dielectric. The electron density is maintained near ~ 1 x 10^{12} cm^{-2} at two different back and front gate voltage combinations.

The magnetoresistivity, shown in figure 2a, was calculated from the measurement of the magnetoresistance at multiple front gate voltages, V_{fg}, while the back gate voltage was fixed at V_{bg} = 0 V and at multiple back gate voltages while the front gate voltage was fixed at V_{fg} = 1 V. A clear beat pattern was observed in the SdH oscillations upon application of gate voltages to the front or back gate, and the beating effect became more pronounced as the potential asymmetry

between front and back gates was increased. The beating was determined to be due to two narrowly separated oscillation frequencies by a Fourier analysis (FA) of the SdH oscillations. The FA is depicted in figure 2b for each of the measurements in figure 2a. The Hall resistances corresponding to the measurements in figure 2a are plotted in figure 2c and 2d.

The electron mobility, μ, exceeded 700,000 cm^2/Vs when the carrier density, N_s, was gated-tuned to ~1.2×10^{12} cm^{-2}, determined from $\mu = 1/\rho_o N_s e$, where ρ_o is the zero magnetic field resistivity and e is the elementary charge. The dependence of mobility on density at several fixed back gate voltages is shown in figure 3a. The density was varied by the front gate voltage. For a given carrier density the mobility could be increased by applying a positive bias to both the front and back gate in comparison to applying a positive bias to only the front gate. This observation can be explained by the creation of a more symmetric quantum well potential for the latter case and a corresponding centered wave function with a reduced scattering rate from rough interfaces. The change in mobility as a function of carrier density has a weaker dependence on back gate voltage at lower carrier density (< 0.6×10^{12} cm^{-2}). The mobility may be limited by scattering mechanisms less sensitive to wave function position in this carrier density regime.

When the 2DEG carrier density was gate tuned to ~ 8×10^{11} cm^{-2}, the onset of SdH oscillations occurred slightly below 0.27 Tesla. This onset corresponds to a Dingle mobility, μ_D, of 37,000 cm^2/Vs and a Dingle temperature, $T_D = e\hbar/(2\pi k_B m^* \mu_D)$, of 1.7 Kelvin. Here, k_B is the Boltzmann constant, and m* the zero-field effective mass. The quantum lifetime of the 2DEG at carrier densities near zero gate voltage was determined using a Dingle analysis of the SdH oscillations[32] over the magnetic field range ~0.6 Tesla to ~1 Tesla. The amplitude of the oscillations, $\Delta\rho$, is given by $\Delta\rho = 4\rho_o X(T)\exp(-\pi/\omega_c\tau_q)$, where ρ_o is the zero-field longitudinal magnetoresistance, and $X(T) = (2\pi^2 k_B T/\hbar\omega_c)/\sinh(2\pi^2 k_B T/\hbar\omega_c)$ is a function of temperature, T,

and $\omega_c = eB/m^*$, where B is the magnetic field. At zero gate bias m* was determined to be $0.032m_o$ from analysis of SdH oscillation amplitudes as a function of temperature. The measurement of the effective mass was in agreement with an estimate using $\mathbf{k}\cdot\mathbf{p}$ formalism accounting for band non-parabolicity[33]. Calculated values were used to account for the effective mass dependence on density. The Dingle analysis at several carrier densities gate-tuned using the back gate is shown in figure 3b along with linear fits to the data. The slight curvature in the Dingle plots with respect to the linear fits may be due to non-parabolicity and competing spin-orbit-coupling and Zeeman effects on the Landau level spectrum. The curvature and the fits' 1/Field = 0 intercepts being greater than 0 may also be due to the presence of a spread in carrier density[34] and field-dependent dephasing. The Dingle analysis does not show evidence of second subband occupation or sample inhomogeneity[34]. The slope of the linear fit provides an estimate of the quantum lifetime at the given carrier density. The quantum lifetime is plotted versus carrier density in figure 3c. The dependence of quantum lifetime on carrier density may be due to a suppression of small-angle-scattering from remote ionized donors upon increasing carrier density[34].

The low magnetic field magnetoresistance oscillations allowed analysis of beat patterns with high frequency resolution. In addition to spin-split subbands, several other mechanisms result in magnetoresistance oscillations with characteristic frequencies; they include magnetophonon resonances (MPR)[35–37] and magneto-intersubband scattering (MIS)[38–40]. Magnetoresistance oscillations characteristic of MPR and MIS were observed when the 2DEG carrier density was gate-tuned above 1.1×10^{12} cm^{-2} in addition to oscillations due to spin-split subbands.

Beat patterns due to spin-split subbands, MPR and MIS were distinguished by measurements of the temperature dependence of the magnetoresistance oscillations and by magnetotransport measurements. MPR and MIS scattering persists in the presence of significant thermal excitation whereas SdH amplitudes decrease rapidly with increasing temperature. The longitudinal magnetoresistance measured at two front gate voltages and at several temperatures for each gate voltage are shown in figure 4a. The FA of the respective magnetoresistance oscillations are shown in figure 4b. At V_{fg} = 1 V and T = 2 Kelvin two narrowly separated oscillation frequencies are observed at $f_{Field} \sim 20$ Tesla. The temperature dependence of the amplitudes of the peaks near 20 Tesla were consistent with the temperature dependence predicted for SdH oscillations. Three additional oscillation frequencies at approximately 12 Tesla, 24 Tesla and 36 Tesla were also observed. The amplitudes of the Fourier peaks located at 12, 24, 36 Tesla slightly decreased or increased as a function of temperature when the front gate was tuned to V_{fg} = 2 V; furthermore, the frequencies of the peaks at 12 and 24 Tesla, which could be resolved at the lower applied gate voltages, were weakly dependent on the gate voltage, suggesting the corresponding oscillations were not due to the SdH effect. The temperature dependence of the Fourier peaks labeled SdH n_+, SdH n_-, 1, 2 and 3 are compared in figure 4c. The amplitudes of SdH n_+ and SdH n_- have a functional dependence on temperature that matches the prediction for SdH oscillations depicted by the solid black line. Fourier peaks 1, 2 and 3 have a weak temperature dependence. Furthermore, when the density was gate-tuned such that the SdH peaks surpassed peak 1 at 36 Tesla, the mobility decreased by approximately 200,000 cm^2/Vs per increase in density by 10^{11} cm^{-2}, suggesting the field at peak 1 corresponds to the MIS fundamental field[40], $f_{Field,\ MIS\ 1} = E_{12}m^*/e\hbar$, where $E_{12} = E_2 - E_1$ is the subband spacing. The

subband spacing determined from the MIS fundamental field is 107 meV. A calculated value for E_{12} is 127 meV. Peaks 2 and 3 are attributed to MPRs.

The narrowly separated SdH oscillation frequencies are interpreted to be due to spin-split subbands. The oscillation frequency of each peak in the FA amplitude provides the population of each spin split subband n_+ and n_- by $n_\pm = e\mathrm{f}_{\mathrm{Field}\pm}/h$. The total carrier density determined by the low field Hall resistance is in good agreement with the density determined by the FA frequencies of the spin-split subbands. Restricting the experiment and analysis to the first occupied subband the Rashba spin orbit coupling parameter is determined by[41]

$$\alpha = \frac{(n_+ - n_-)\hbar^2}{m^*}\sqrt{\frac{\pi}{2N_S - 2(n_+ - n_-)}}. \quad (1)$$

The experimentally determined Rashba spin orbit coupling parameter, α, versus carrier density measured at a multiple back gate and front gate voltage combinations is shown in figure 5. The data is grouped by a common fixed front gate voltage. For a given front gate voltage the density was changed by varying the back gate voltage from 0 V to -1.0 V in 0.2 V increments. An increase in the difference between the back and front gate voltages generated an increase in α, and α could be increased at constant carrier density by appropriate set points of the back and front gate voltages.

The expectation value of the electric field, $\langle E \rangle$, over the quantum well varied between 20 kV/cm and 50 kV/cm for gate voltage combinations having the lowest and highest potential asymmetry, respectively. A scaling factor, b, that parameterizes the spin-orbit interaction parameter, $\alpha = b\langle E \rangle$, at constant carrier density was approximately 170 eÅ^2 electric quadrupole moments. This value is notably larger than the electric field contribution of the spin-splitting

parameter resulting from the quantum well alone[42], which is calculated to be 120 eÅ^2 for the InAs/AlSb quantum well under investigation, and suggests interface contributions to the zero-field spin-splitting energy were significant.

The strong dependence of α on the gate-controlled potential asymmetry suggests the structure inversion asymmetry contribution to the total spin orbit interaction was controlled by the Rashba mechanism. This finding is in contrast with previous results[24,25]; however, by using 2DEGs with exceptionally high mobility and implementing electric field control by integrating both a back and front gate this work was able to resolve finer changes in the spin splitting energy and probe a previously unexplored range of potential asymmetry and carrier density in this system. In addition to offering technological advances for studies in Spintronics and related fields, the back and front gated high mobility 2DEG confined to the InAs/AlSb heterostructure enables the investigation of a system wherein phenomena inherent to high carrier mobility two-dimensional semiconductors and to narrow band gap semiconductors with tunable spin-orbit coupling coexist.

This work has demonstrated the gate control of zero field spin-splitting in a high quality back and front gated InAs-AlSb heterostructure. Magnetotransport experiments on a high mobility 2DEG confined to the InAs channel showed clean Shubnikov de Haas oscillations down to low magnetic fields. Analysis of the magnetoresistance oscillations indicated the spin-splitting energy in the first subband was controlled by front and back gates via the Rashba effect. The spin-splitting energy could be modified while keeping the 2DEG charge density constant.

Acknowledgements

This work was supported by Microsoft Research Station Q. This work made use of the central facilities of the UCSB MRL, which is supported by the MRSEC program of the National Science Foundation under Award No. DMR-1121053. This work also made use of the UCSB Nanofabrication Facility, a part of the NSF funded NNIN network, and of the California NanoSystems Institute. The authors thank David D. Awschalom for assistance with measurements.

References

[1] Y.A. Bychkov and E.I. Rashba, J. Phys. C Solid State Phys. **17**, 6039 (1984).

[2] S. Datta and B. Das, Appl. Phys. Lett. **56**, 665 (1990).

[3] I. Žutić, J. Fabian, and S. Das Sarma, Rev. Mod. Phys. **76**, 323 (2004).

[4] D.D. Awschalom and M.E. Flatte, Nat. Phys. **3**, 153 (2007).

[5] A. Manchon, H.C. Koo, J. Nitta, S.M. Frolov, and R.A. Duine, Nat. Mater. **14**, 871 (2015).

[6] P. Debray, S.M.S. Rahman, J. Wan, R.S. Newrock, M. Cahay, A.T. Ngo, S.E. Ulloa, S.T. Herbert, M. Muhammad, and M. Johnson, Nat. Nanotechnol. **4**, 759 (2009).

[7] M. Kohda, S. Nakamura, Y. Nishihara, K. Kobayashi, T. Ono, J. Ohe, Y. Tokura, T. Mineno, and J. Nitta, Nat. Commun. **3**, 1082 (2012).

[8] S. Nadj-Perge, S.M. Frolov, E.P.A.M. Bakkers, and L.P. Kouwenhoven, Nature **468**, 1084 (2010).

[9] K.D. Petersson, L.W. McFaul, M.D. Schroer, M. Jung, J.M. Taylor, A.A. Houck, and J.R. Petta, Nature **490**, 380 (2012).

[10] J. Wunderlich, B.-G. Park, A.C. Irvine, L.P. Zârbo, E. Rozkotová, P. Nemec, V. Novák, J. Sinova, and T. Jungwirth, Science **330**, 1801 (2010).

[11] P. Chuang, S.C. Ho, L.W. Smith, F. Sfigakis, M. Pepper, C.H. Chen, J.C. Fan, J.P. Griffiths, I. Farrer, H.E. Beere, G.A.C. Jones, D.A. Ritchie, and T.M. Chen, Nat. Nanotechnol. **10**, 35 (2014).

[12] J.D. Sau, R.M. Lutchyn, S. Tewari, and S. Das Sarma, Phys. Rev. Lett. **104**, 040502 (2010).

[13] J. Alicea, Phys. Rev. B **81**, 125318 (2010).

[14] R.M. Lutchyn, J.D. Sau, and S. Das Sarma, Phys. Rev. Lett. **105**, 077001 (2010).

[15] Y. Oreg, G. Refael, and F. von Oppen, Phys. Rev. Lett. **105**, 177002 (2010).

[16] J.D. Sau, S. Tewari, and S. Das Sarma, Phys. Rev. B **85**, 064512 (2012).

[17] G. Dresselhaus, Phys. Rev. **100**, 580 (1955).

[18] G. Lommer, F. Malcher, and U. Rossler, Phys. Rev. Lett. **60**, 728 (1988).

[19] R. Winkler, *Spin Orbit Coupling Effects in Two-Dimensional Electron and Hole Systems* (Springer, Berlin, 2003).

[20] J. Nitta, T. Akazaki, H. Takayanagi, and T. Enoki, Phys. Rev. Lett. **78**, 1335 (1997).

[21] D. Grundler, Phys. Rev. Lett. **84**, 6074 (2000).

[22] T. Koga, J. Nitta, T. Akazaki, and H. Takayanagi, Phys. Rev. Lett. **89**, 046801 (2002).

[23] J.B. Miller, D.M. Zumbühl, C.M. Marcus, Y.B. Lyanda-Geller, D. Goldhaber-Gordon, K. Campman, and a C. Gossard, Phys. Rev. Lett. **90**, 076807 (2003).

[24] J.P. Heida, B.J. van Wees, J.J. Kuipers, T.M. Klapwijk, and G. Borghs, Phys. Rev. B **57**, 11911 (1998).

[25] S. Brosig, K. Ensslin, R. Warburton, C. Nguyen, B. Brar, M. Thomas, and H. Kroemer, Phys. Rev. B **60**, R13989 (1999).

[26] B. Shojaei, A. Mcfadden, J. Shabani, B.D. Schultz, and C.J. Palmstrøm, Appl. Phys. Lett **106**, 222101 (2015).

[27] G. Tuttle, H. Kroemer, and J.H. English, J. Appl. Phys. **67**, 3032 (1990).

[28] D. Nečas and P. Klapetek, Cent. Eur. J. Phys. **10**, 181 (2012).

[29] I.H. Tan, G.L. Snider, L.D. Chang, and E.L. Hu, J. Appl. Phys. **68**, 4071 (1990).

[30] I. Vurgaftman, J.R. Meyer, and L.R. Ram-Mohan, J. Appl. Phys. **89**, 5815 (2001).

[31] M.L. Huang, Y.C. Chang, C.H. Chang, T.D. Lin, J. Kwo, T.B. Wu, and M. Hong, Appl. Phys. Lett. **89**, 012903 (2006).

[32] P.T. Coleridge, R. Stoner, and R. Fletcher, Phys. Rev. B **39**, 1120 (1989).

[33] E.O. Kane, J. Phys. Chem. Solids **1**, 249 (1957).

[34] P.T. Coleridge, Phys. Rev. B **44**, 3793 (1991).

[35] V.L. Gurevich and Y.A. Firsov, J. Exp. Theor. Phys. **13**, 137 (1961).

[36] D.C. Tsui, T. Englert, A.Y. Cho, and A.C. Gossard, Phys. Rev. Lett. **44**, 341 (1980).

[37] M.A. Zudov, I. V. Ponomarev, A.L. Efros, R.R. Du, J.A. Simmons, and J.L. Reno, Phys. Rev. Lett. **86**, 3614 (2001).

[38] M. Raikh and T. Shahbazyan, Phys. Rev. B **49**, 5531 (1994).

[39] A.C.H. Rowe, J. Nehls, and R.A. Stradling, Phys. Rev. B **63**, 201307 (2001).

[40] T.H. Sander, S.N. Holmes, J.J. Harris, D.K. Maude, and J.C. Portal, Phys. Rev. B **58**, 13856 (1998).

[41] G. Engels, J. Lange, T. Schapers, and H. Luth, Phys. Rev. B **55**, 1958 (1997).

[42] E.A. de Andrada e Silva, G.C. La Rocca, and F. Bassani, Phys. Rev. B **50**, 8523 (1994).

Figures

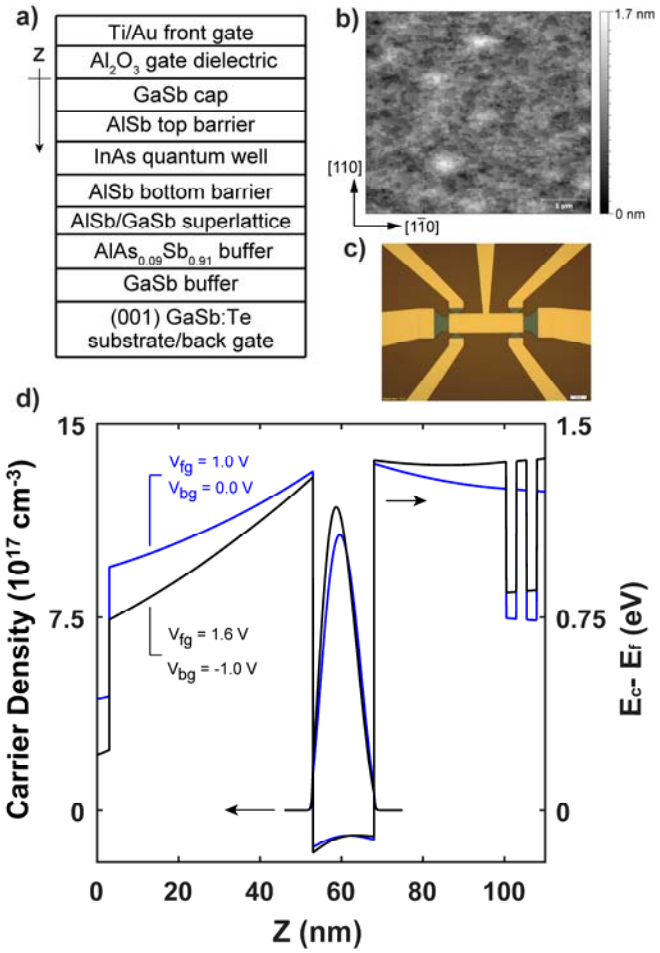

Figure 1. (a) A schematic of the InAs quantum well heterostructure with Al_2O_3 gate dielectric and Ti/Au front gate. (b) A 5 μm x 5 μm atomic force microscope image of the heterostructure taken at the surface of the GaSb capping layer. (c) An optical micrograph of the Hall bar used in this study. The scale bar at the lower right represents 20 μm. (d) A self-consistent calculation of the conduction band profile and carrier density distribution in the vicinity of the InAs quantum well when V_{fg} = 1 V and V_{bg} = 0 V (blue lines), and when V_{fg} = 1.6 V and V_{bg} = -1 V (black lines). See text for details of the calculation.

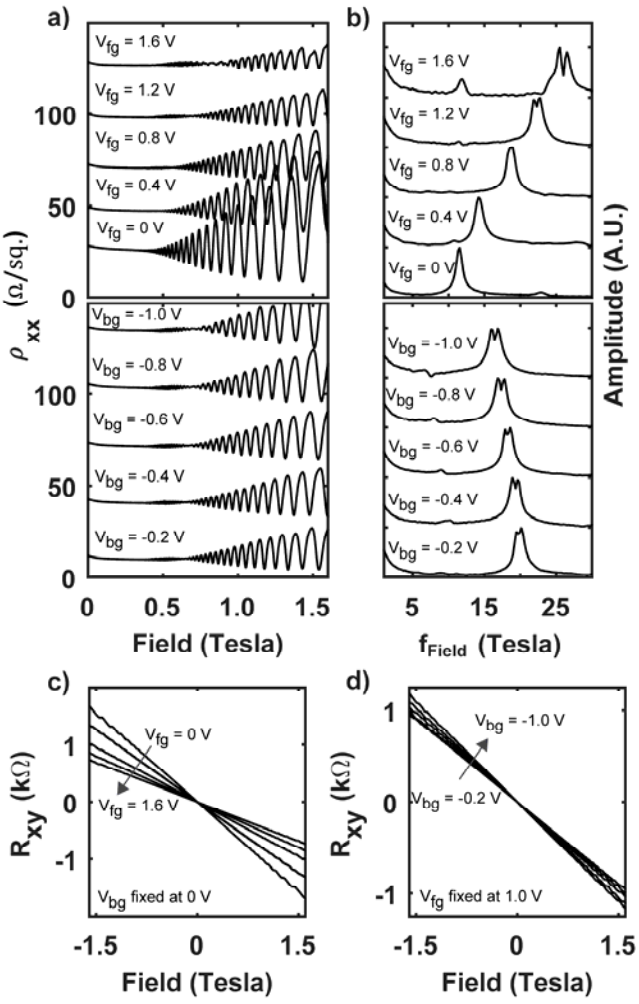

Figure 2. (a) Magnetoresistivity at V_{fg} = 0, 0.4, 0.8, 1.2, and 1.6 V while V_{bg} = 0 V (upper plot), and at V_{bg} = -0.2, -0.4, -0.6, -0.8 and -1 V while V_{fg} = 1 V (lower plot). (b) Fourier amplitude versus magnetoresistance oscillation frequency determined from a Fourier analysis of the corresponding magnetoresistance in (a) as a function of inverse magnetic field. The data in (a) and (b) are offset for clarity. (c) Hall resistance at V_{fg} = 0, 0.4, 0.8, 1.2, and 1.6 V while V_{bg} = 0 V. (d) Hall resistance at V_{bg} = -0.2, -0.4, -0.6, -0.8 and -1 V while V_{fg} = 1 V. Measurements were performed at a sample temperature of 2 Kelvin.

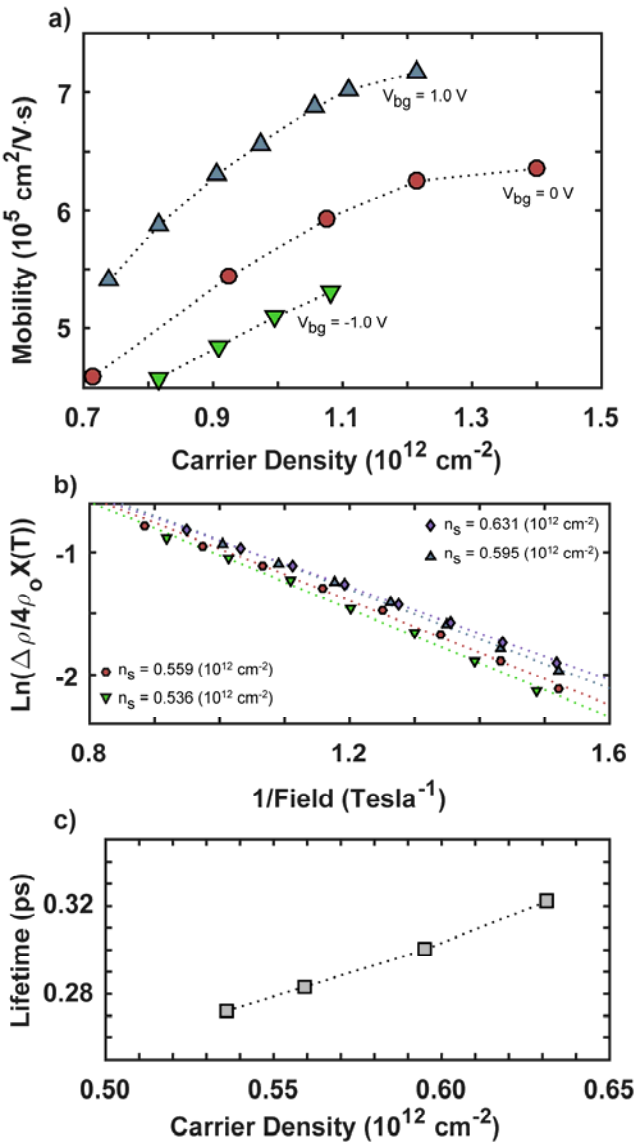

Figure 3. (a) The dependence of mobility on carrier density at a sample temperature of 2 Kelvin and at constant back gate voltages V_{bg} = -1 V, V_{bg} = 0 V and V_{bg} = +1 V. The carrier density was varied using the front gate, where in each case an increase in the front gate voltage corresponds to an increase in carrier density. (b) Dingle analysis of the SdH oscillations at a sample temperature of 2 Kelvin and at four carrier densities near zero gate bias. The carrier density was modulated using the back gate. Linear fits are shown as dotted lines. (c) The dependence of quantum lifetime on carrier density determined from the data in (b).

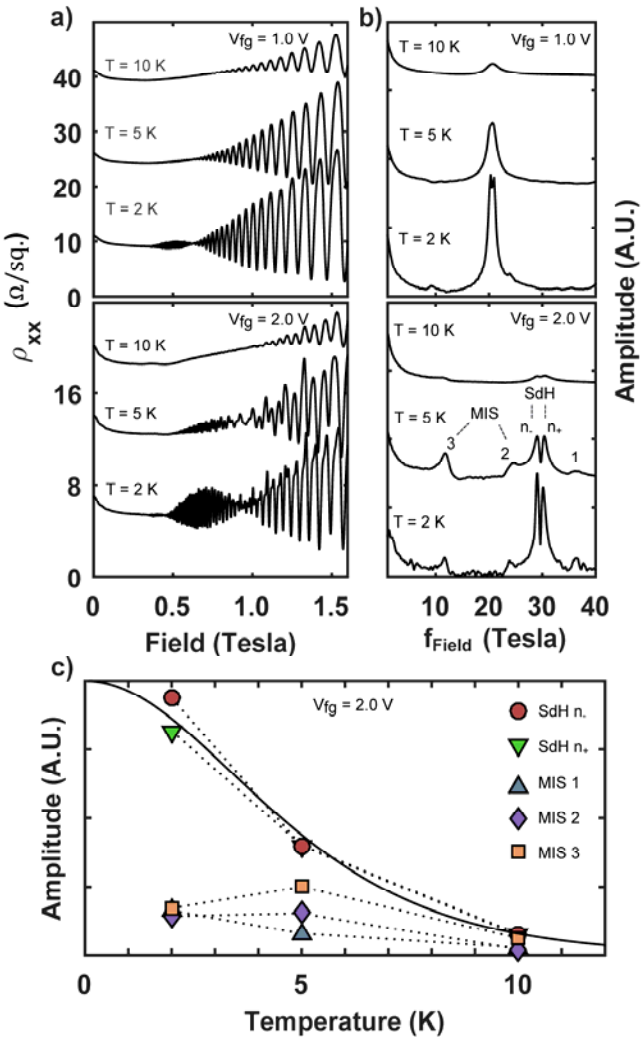

Figure 4. (a) Magnetoresistivity at sample temperatures 2, 5 and 10 Kelvin for V_{fg} = 1.0 V (upper plot) and V_{fg} = 2.0 V (lower plot). (b) Fourier amplitude versus magnetoresistance oscillation frequency determined from a Fourier analysis of the corresponding magnetoresistance in (a) as a function of inverse magnetic field. The data in (a) and (b) are offset for clarity. (c) The temperature dependence of the Fourier amplitudes denoted by SdH n_+, SdH n_-, 1, 2 and 3 in the Fourier analysis shown in (b) for the front gate voltage, V_{fg} = 2 V. The solid line depicts the theoretical temperature dependence of SdH Fourier amplitudes, $\sim (2\pi^2 k_B T/\hbar\omega_c)/\sinh(2\pi^2 k_B T/\hbar\omega_c)$.

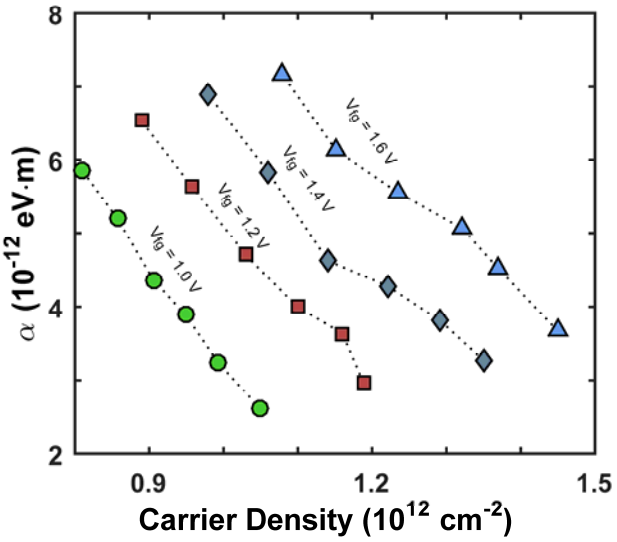

Figure 5. Experimentally determined Rashba spin orbit coupling parameter versus carrier density. The data is grouped by common fixed front gate voltage. For a given front gate voltage the back gate voltage was varied from 0 V to -1.0 V in 0.2 V increments.